Proceedings of ASME Turbo Expo 2011
GT2011
June 6-10, 2011, Vancouver, British Columbia, Canada

GT2011-45106

EXPERIMENTAL AND NUMERICAL INVESTIGATION OF FLOW FIELD AND DOWNSTREAM SURFACE TEMPERATURES OF CYLINDRICAL AND DIFFUSER SHAPED FILM COOLING HOLES

Tilman auf dem Kampe, Stefan Völker
Fossil Power Generation Division
Siemens AG, Energy Sector
45473 Mülheim a. d. Ruhr, Germany
Email: tilman.aufdemkampe@siemens.com

Torsten Sämel
Institut für Strömungsmechanik
Technische Universität Dresden
01062 Dresden, Germany

Christian Heneka, Helge Ladisch, Achmed Schulz, Hans-Jörg Bauer
Institut für Thermische Strömungsmaschinen
Karlsruhe Institute of Technology
76131 Karlsruhe, Germany

ABSTRACT

An experimental and numerical study of the flow field and the downstream film cooling performance of cylindrical and diffuser shaped cooling holes is presented.

The measurements were conducted on a flat plate with a single cooling hole with coolant ejected from a plenum. The flow field was investigated by means of 3D-PIV as well as 3D-LDV measurements, the downstream film cooling effectiveness by means of infrared thermography. Cylindrical and diffuser holes without lateral inclination have been examined, varying blowing ratio and density ratio as well as freestream turbulence levels. 3D-CFD simulations have been performed and validated along with the experimental efforts.

The results, presented in terms of contour plots of the three normalized velocity components as well as adiabatic film cooling effectiveness, clearly show the flow structure of the film cooling jets and the differences brought about by the variation of hole geometry and flow parameters. The quantitative agreement between experiment and CFD was reasonable, with better agreement for cylindrical holes than for diffuser holes.

NOMENCLATURE

Latin Symbols

A	Cross section area
AR	Diffuser area ratio
d	Hole diameter
DR	Density ratio
h	Heat transfer coefficient
L	Hole length
M	Blowing ratio
$\dot{m}$	Mass flow
Ma	Mach number
$\dot{q}$	Heat flux
t/P	Hole coverage
T	Temperature
Tu	Turbulence intensity
u,v,w	Velocity components
x,y,z	Cartesian coordinates

Greek Symbols

α	Inclination angle
δ	Boundary layer thickness
ε	Emissivity
η	Film cooling effectiveness
λ	Thermal conductivity
ρ	Density

Subscripts

aw	Adiabatic wall conditions
c	Coolant conditions
$cond$	Conduction
$conv$	Convection
f	With film cooling
$inlet$	Cooling hole inlet
lat	Laterally averaged values
m	Hot gas conditions
$outlet$	Cooling hole outlet

rad	Radiation
rec	Recovery influence
ref	Reference value
t	Total
w	Wall

INTRODUCTION

Film cooling is one of the most important cooling technologies for gas turbine vanes and blades. Although it has been used for decades, its potential to help increase turbine inlet temperatures and thus engine efficiency and output is still significant. Since film cooling is unfavorable from a thermodynamic cycle point of view, a highly efficient use of film cooling is called for. Due to its great potential many studies have been undertaken to improve the understanding of film cooling flows and the way they interact with the hot gas flow in an attempt to find means to leverage the greatest possible benefit from film cooling.

A large number of experimental investigations dealing with both the aerodynamic as well as the thermal aspect of film cooling by discrete holes were published over the past 40 years, most of them using flat plate tests to isolate the effect of the relevant parameters. The study of Goldstein et al. [1] is considered to be the first to consistently measure the effectiveness of cylindrical film cooling holes inclined to the surface. Further measurements, including variations of hole parameters such as the compound angle and the hole shape, are presented in Goldstein et al. [2] and Goldstein et al. [3]. Also, the advantages of fanshaped holes over cylindrical holes have been documented. The coolant momentum at the hole exit is reduced due to the diffusion inside the hole. Thus the coolant remains close to the surface without any tendency to lift off, which becomes a problem for cylindrical holes at high blowing ratios. Furthermore, the lateral expansion of the hole contour leads to an improved lateral coverage downstream of the hole exit, allowing the reduction of the number of holes.

Although the advantage of shaped holes is undisputed, a significant number of studies still focuses on cylindrical holes. The most relevant geometric properties include inclination angle (Foster and Lampard [4], Baldauf et al. [5], and Baldauf et al. [6]), compound angle (Schmidt et al. [7], Ligrani et al. [8], and Goldstein and Jin [9]), and length to diameter ratio (Lutum and Johnson [10] and Burd et al. [11]). Concerning shaped film cooling holes, various diffuser shapes have been tested over a wide range of internal and external boundary conditions. Recently an overview over the corresponding studies was given by Bunker [12]. Gritsch et al. [13] compared two types of shaped cooling holes with a cylindrical hole. Both shaped holes - a fanshaped hole with a lateral expansion only and a laidback fanshaped hole with a lateral and forward expansion - substantially outperformed the cylindrical hole in terms of cooling efficiency. The effect of different expansion angles of the diffuser part were tested extensively by Saumweber and Schulz [14] for fanshaped holes and by Gritsch et al. [15] for laidback fanshaped holes. Additional parameters such as compound angle, area ratio and inclination angle of laidback fanshaped holes are discussed in Heneka et al. [16].

Up to now little data has been presented dealing with high resolution aerodynamic measurements. As CFD calculations of cooling configurations become more and more common, such measurements are essential to validate CFD predictions. Results of aerodynamic tests using LDV have been presented by Pietrzyk et al. [17] for cylindrical holes. However only two-dimensional centerline data was measured. Therefore, the lateral spreading of the coolant was not quantified. Using 2D LDV measurements, Thole et al. [18] compared velocity maps inside and downstream of the hole for two different diffuser geometries with those of a cylindrical hole. Flowfield measurements downstream of cylindrical holes by means of five-hole probes were conducted in an in-line arrangement by Lee et al. [19] and with compound angle by Lee et al. [20]. Their measurements underlined the three-dimensional characteristics of the film cooling flow similar to a jet-in-crossflow. PIV measurements in the downstream region of cylindrical holes at different blowing ratios and density ratios were presented by Jessen et al. [21]. In this study the developement of the typical counterrotating vortex pair was described, which is present even in case of laidback fanshaped shaped holes, given the area ratio between exit and inlet cross section of the hole is small (Jessen et al. [22]).

Besides experimental film cooling investigations, there is a broad range of film cooling CFD literature. A fairly complete film cooling CFD bibliography, covering a quarter of a century from 1971 through 1996, was presented by Kercher [23] in 1998. The aforementioned bibliography contains references to almost 200 papers and dissertations. Since then the frequency of film cooling related publications has increased significantly due to the growing interest in film cooling technology and the rapid growth of computational power.

Some publications related to 3D-CFD of film cooling flows aimed at providing best practice guidelines for applying 3D-CFD methodology and to evaluate its predictive capability. Leylek and Zerkle [24] were among the first to consider CFD predictions of the flow field downstream of the cooling hole exit. Later, Walters and Leylek [25] suggested a systematic computational methodology for numerical simulation of film cooling flows, based on which Walters and Leylek [26] and Hyams and Leylek [27] then executed a detailed analysis of cylindrical and shaped hole film cooling with streamwise injection. The investigators highlighted the importance of including the cooling hole and its inflow region in the CFD analysis as the characteristic counter-rotating vortex pair is initiated by the turning and acceleration of the flow at hole inlet (“jetting effect”). Including hole and plenum has become the standard for film cooling CFD simulations. The investigators

also found that RANS-based turbulence models tend to underpredict lateral spreading of film cooling jets, which in turn leads to an overprediction of centerline effectiveness. Considering lateral averages of film cooling effectiveness, however, CFD predictions can deliver reasonable results. A lot of research is aimed at improving turbulence modeling specifically for film cooling. Bacci and Facchini [28], for example, presented an anisotropic turbulence model for the numerical simulation of film cooling flows.

Other investigators used 3D-CFD to evaluate various types of cooling hole geometries or other geometrical features to positively influence the cooling effectiveness (see Shih and Na [29], Na and Shih [30], or Lee and Kim [31]).

Flat plate calculations dominated the 3D-CFD analyses in the past as they allow one to analyze various influencing factors separately. The importance of plenum cross-flow and internal channel geometry for example has received more attention in recent years and has often been investigated, both by means of experimental and numerical investigations (Kissel et al. [32]). However, with increasing computational resources, researchers have successfully applied 3D-CFD to simulate entire gas turbine components including film cooling (Colban et al. [33], Goormans-Francke et al. [34]). It is obvious though that complex 3D-CFD models of entire gas turbine components including film cooling flows are still very demanding in terms of computational resources, especially if highly accurate predictions of surface temperature and heat transfer are sought after.

To alleviate the resource requirements, another branch of film cooling CFD research aims at the development of simplified film cooling models. Among the first proposals for a film cooling model is the 2D approach proposed by Miller and Crawford [35]. For 3D-CFD, Heidmann and Hunter [36] proposed using volumetric source terms. Burdet et al. [37] developed an injection model using immersed boundary conditions to model the extent of the film cooling jet and its blockage effect to the approach flow. Tartinville and Hirsch [38] also proposed an injection based model. Auf dem Kampe and Völker [39] employed distributed volumetric source terms to model cylindrical hole film cooling flows.

The study presented in this paper focuses on improving the understanding of the flow physics of jet and cross-flow interaction as well as to provide a validated, detailed CFD model for both cylindrical and diffuser shaped film cooling holes. Its novel feature is the detailed three-dimensional analysis of the flow field together with adiabatic wall temperature measurements downstream of cylindrical and diffuser shaped cooling holes. It combines an experimental analysis of the flow field with CFD computations. The validated, detailed CFD model provides the basis for the development of a correlation for diffuser shaped hole film cooling flows similar to the correlation presented for cylindrical holes by auf dem Kampe and Völker [40] and auf dem Kampe et al. [41]. CFD validation for previous investigations was based on surface temperatures only, the present study includes a detailed experimental investigation of the film jet flow field.

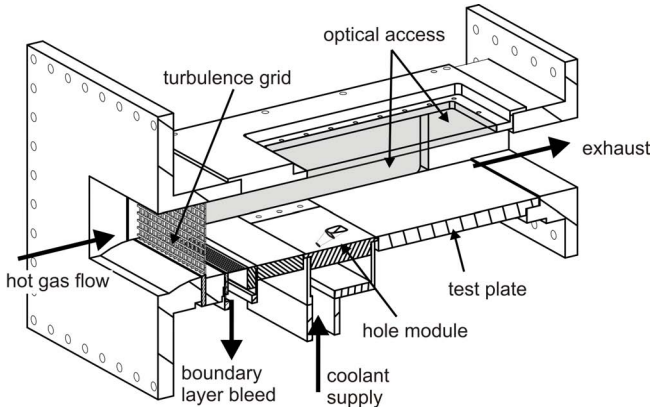

FIGURE 1. Schematic view of test section

EXPERIMENTAL SETUP

The experimental investigations were performed in a subsonic test facility at the Institute of Thermal Turbomachinery (ITS) at Karlsruhe Institute of Technology (KIT). A flat plate test rig was used with a single cooling hole with coolant ejected from a plenum. The air flow representing the external hot gas flow is supplied by a radial compressor, heated up to the required temperature by an electrical heater and led to the rectangular test section via flow straighteners, grids and a high contraction nozzle. The dimension of the test section is 105mm in height and 200mm in width. At the entrance to the test section turbulence grids can be inserted to allow for adapting the turbulence intensity. A boundary layer bleed is included to control the boundary layer thickness. Windows at the side walls and the top wall of the test rig provide optical access to the test section (Figure 1). The air flow representing the coolant flow is supplied by a second blower. The coolant mass flow is measured by a mass flow meter before entering the coolant cavity. The dimension of the cavity is such that plenum condition can be assumed at the entrance of the tested film cooling holes. The coolant is ejected through a single cooling hole. Downstream of the coolant ejection module, which is manufactured stereolithographically out of Prototool, different test plates have been placed allowing for the different measurement techniques. For the aerodynamic measurements a simple plate made of stainless steel was used. For the thermal measurements test plates made of Tecapeek, a plastic material with a very low thermal conductivity, were used to approximate near adiabatic conditions. All test plates have been covered with black coating to reduce Laser light reflection and to ensure constant emissivity ($\varepsilon = 0.95$), which is crucial for infrared techniques.

The external Mach number has been kept constant at $Ma = 0.185$. Hence the Reynolds number based on the hole inlet diam-

TABLE 1. Operating conditions

Hot gas Mach number	Ma	0.185
Hot gas temperature	$T_{t,m}$	330K, 420K
Coolant temperature	$T_{t,c}$	298K
Hot gas turbulence intensity	Tu	1.5%, 7%
Boundary layer thickness	δ_1/d	0.1
Blowing ratio	M	0.5-2.0
Density ratio	DR	1.1, 1.4

eter is between $2 \cdot 10^4$ and $3 \cdot 10^4$, as it is typical for high pressure turbine film cooling. The hot gas static pressure is measured by means of a pressure tap, the total pressure by means of a Pitot probe. A thermocouple is inserted into the Pitot probe to detect the hot gas total temperature. The freestream turbulence intensity and the thickness of the approaching boundary layer were measured at the location of the hole exit prior to the film cooling experiments using constant temperature anemometry. The freestream temperature is limited by the maximum temperature of the hole module material. Thus two density ratios were investigated ($DR = 1.1$ and 1.4). The blowing ratio was varied between $M = 0.5 - 2.0$). It was calculated using the measured total coolant mass flux $\dot{m}_c$ and the cylindrical inlet cross section A_{inlet}. The entire operating conditions are listed in Table 1.

Film cooling configurations:

The two tested hole geometries feature an inclination angle of 35° and are aligned parallel to the hot gas flow. The diffuser part of the laidback fanshaped hole opens 10° in lateral and forward direction after a cylindrical inlet section with a diameter of d and a length of $2d$. The diffuser corners are rounded. The overall length of the diffusor hole is identical to the cylindrical hole resulting in an area ratio (defined as the ratio of the exit cross section $A_{outlet}$to the cylindrical inlet cross section A_{inlet}, cp. Fig. 2) of $AR = 3.71$.

MEASUREMENT TECHNIQUE

Aerodynamic investigations:

To analyse the flow field at the exit region of the cooling holes, 3-dimensional PIV measurements have been performed. The Laser light sheet is applied through the top window into the test rig. Two CCD cameras with a resolution of 1280×1024 pixels have been positioned at the front side and the back side of the test rig at a relative angle to the light sheet plane to allow a stereoscopic PIV analysis. The whole optical hardware is assembled on a traversing system, enabling measurements at different lateral positions. Both the hot gas and the coolant flow are seeded with oil particles (DES) with a mean diameter of approx. 0.5μm. For each hole geometry tested, measurements have been conducted in 21-25 lateral planes over the whole outlet area of the hole exit portions. For the recording of the pictures and the elementary post processing steps (stereo cross correlation) the commercial software Davis (V7.1, LaVision) has been used. Further post processing steps have been done using Matlab, finally resulting in a fully volumetric 3D vector field.

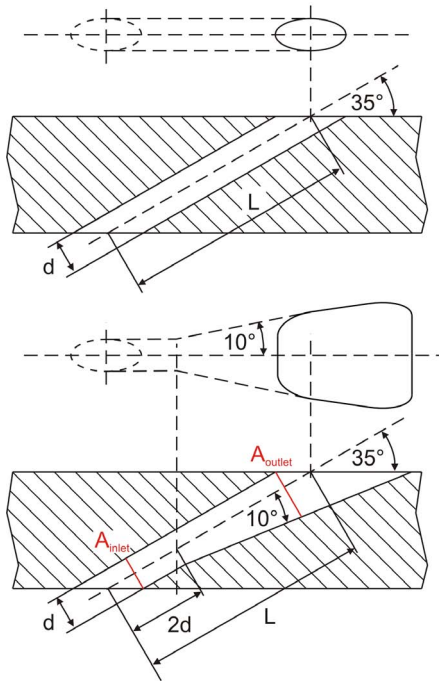

FIGURE 2. Film cooling hole geometries

Additional LDV measurements have been performed to get time resolved data allowing for the calculation of turbulent quantities. A three-component, fiber optic laser Doppler velocimeter was used to measure velocity profiles at various positions downstream of the hole exit coincidentally. An argon-ion laser and a subsequent splitter box emit three pairs of Laser beams (478.5, 488, 512nm) allowing for the detection of three velocity components. The LDV system consists of two fiber optic probes with a focal length of 400mm and Enhanced Burst Spectrum Analyzers. As in the case of PIV tests, both the hot gas and the coolant flow were seeded with oil particles. The two probes were positioned at the front and the back side of the test rig taking advantage of the improved intensity of forward scattering arrangement. They were aligned at a relative angle to enable 3D-analysis. The subsequent correction to cartesian coordinates has been done using Matlab.

Thermal investigations:

For the description of the thermal characteristics of film cooling ejection the adiabatic film cooling effectiveness is used. It is defined according to:

$$\eta_{aw} = \frac{T_{rec,m} - T_{aw}}{T_{rec,m} - T_{t,c}} \tag{1}$$

The coolant temperature $T_{t,c}$ has been measured inside of the coolant cavity before the entrance of the film cooling holes. The hot gas temperature $T_{rec,m}$ is derived from the hot gas total temperature. As the adiabatic wall temperature T_{aw} is not measurable directly, it has been gained from one experiment with near adiabatic wall conditions according to Eq. 2 using a test plate material (Tecapeek) with a very low thermal conductivity of $\lambda = 0.25\frac{\mathrm{W}}{\mathrm{mK}}$.

$$T_{aw} = T_w + \frac{\dot{q}_{conv}}{h_f} \tag{2}$$

The heat transfer coefficient h_f is taken from a flat plate correlation for turbulent flows by Kays et al. [42]. The temperature T_w of the wall downstream of the coolant ejection has been measured using an infrared camera. The camera system (FLIR SC6000) features an excellent spatial resolution of 640x512pixels at approx. 0.5mm^2 per pixel. An edge filter cutting wavlengths beyond 4.0μm is used to minimize the influence of the radiation of the hot sapphire window. Hence heat radiation is detected between 3.0 and 4.0μm. The test plate is coated with black velvet coating leading to a constant emissivity of $\varepsilon = 0.95$ over a wide range of viewing angles. To increase the accuracy of the wall temperature measurement a number of thermocouples are distributed over the test plates which are used for an in-situ calibration. The general approach is described in detail in Martiny et al. [43] and Schulz [44]. An advancement of this approach has been presented recently by Ochs et al. [45]. They integrated the underlying physics of heat radiation and camera detector features into the approach leading to a more robust system. Furthermore, this new approach needs much fewer thermocouples. The resulting two dimensional temperature distribution of the test plate surface and an interpolated distribution gained from thermocouple readings on the backside serve as boundary conditions of a finite volume calculation of the heat flux within the test plates. To derive the convective heat flux, the calculated conductive heat flux is corrected by the radiative heat flux resulting from a surface to surface radiation simulation (Eq. 3).

$$\dot{q}_{conv} = \dot{q}_{cond} - \dot{q}_{rad} \tag{3}$$

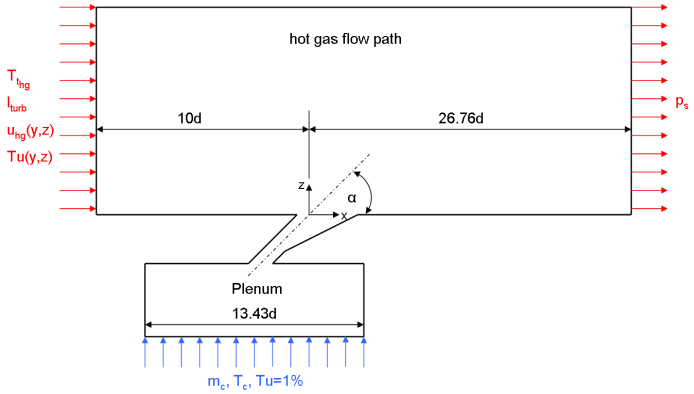

FIGURE 3. Computational domain and boundary conditions

By using the material Tecapeek with a low thermal conductivity the maximum correction to adiabatic conditions according to Eq. 2 for all test cases amounts to 5K implying a minor effect of the simplifying approximations of $\dot{q}_{conv}$ and h_f.

MEASUREMENT UNCERTAINTIES

In the following, maximum uncertainties of the experimental results are given. For results coming from PIV measurements the uncertainty of the velocity components aligned with the light sheet can be estimated to about 2% outside the boundary layer and to about 5% inside the boundary layer. The velocity component normal to the light sheet is calculated from the 2D vector field results of the 2 cameras leading to an uncertainty of about 4% outside the boundary layer and to about 8% inside the boundary layer. Near wall velocities are additionally influenced by occurring reflections of the Laser light sheet, increasing the uncertainties to about 10% in this region. Concerning the results of the LDV measurements a maximum error of $\pm 1 m/s$ can be estimated resulting from the uncertainty in determining the angles of the probes' axes which affect the conversion into cartesian coordinates. The uncertainty in measuring the individual temperatures is below 1K. The distribution of the convective heat flux results from numerical calculations, the heat transfer coefficient from a flat plate correlation. With this approximations the uncertainty determining the adiabatic wall temperature T_{aw} can be calculated to 2K max. Using the approach given by Kline and McClintock [46] the uncertainty of the adiabatic film cooling effectiveness can be calculated to 6%.

CFD SETUP

The computational domain matched the geometrical extent of the experimental test rig and can be separated into three parts: Hot gas flow path, cooling hole, and plenum (Figure 3). The flow path width was set to 36.42d corresponding to the experimental

test rig. The inlet was located $10d$ upstream, the outlet $26.76d$ downstream of the coolant injection. The film cooling hole with a 35 degree inclination angle (Figure 2) and a streamwise orientation connects plenum and hot gas flow path. The plenum was modeled large enough to ensure no interaction between plenum inlet and film cooling hole inlet and had a width of $24d$.

All walls were treated as adiabatic, no slip walls. Inlet temperature, velocity and turbulence distributions were obtained from measurements, while the inlet turbulence length scale was set to approximately $2d$ to match the measured turbulence decay in the test rig. The measured inlet velocity and turbulence distributions in wall normal and lateral direction were interpolated onto the inlet surface. The average free stream turbulence intensity at the inlet was 1% and 7%, respectively. A measured static pressure was specified for the hot gas flow path outlet. Depending on the blowing ratios different mass flow rates at ambient temperature were applied at the plenum inlet. The boundary conditions like density ratio, blowing ratio, pressure etc. were adapted for each case using the exact experimental boundary conditions. A low turbulence intensity of 1% was assumed for the flow at plenum inlet.

The computational mesh was generated using the commercial software CENTAUR_Plus 9.0.2 by CentaurSoft for hybrid unstructured mesh generation. The mesh consisted of tetrahedra and prism layers. Local refinement in the vicinity of the film hole exit and film hole inlet ensured sufficient mesh density for resolving small length scale secondary flows. The boundary layers on the platform, inside the hole and on the plenum top wall were meshed with prism layers, which form a continuous surface. A y^+ value of unity was achieved in the relevant areas. The computational grid was sufficiently fine to resolve the inhomogeneities in the approach flow. Due to the distance between film cooling hole and flow path side walls, top wall and plenum side walls were not resolved with prism layers in order to reduce node count and, therefore, computation time. Mesh sizes varied from 2.7 to 3.1 million nodes for cylindrical and shaped cooling hole geometries.

The simulation was performed using the commercial flow solver ANSYS CFX, which is an implicit pressure-based algorithm using a conservative finite element-based control volume method. In order to capture small gradients, a second order discretization scheme for all variables with an automatic pseudo time scale for the steady state calculation was applied. The turbulence was modeled using the k-ω-SST model of Menter [47] with reattachment modification and low Reynolds number models for the near wall treatment. Solutions were considered converged when RMS residuals for each transport quantity (mass, momentum, energy, turbulent kinetic energy and turbulent eddy frequency) had decreased by at least two orders of magnitude and remained approximately constant for at least 50 iterations, while domain imbalances for each transport quantity were below 1%.

RESULTS

In this section a comparison of experimental results with computational simulations is presented for a cylindrical and a diffuser shaped film cooling hole. Both geometries feature a 35 degree inclination angle and coolant injection parallel to the main stream flow direction. Both cylindrical and shaped hole were investigated at identical operating points. For the shaped hole, a second operating point at elevated blowing ratio was investigated. All experiments and the corresponding simulations were performed with a constant main stream Mach number of $Ma = 0.185$.

Cylindrical Film Cooling Hole

Case 1: $\alpha = 35^\circ$, $M = 1.0$, $DR = 1.4$, $Tu = 7\%$

The dominant secondary flow structure for inclined cylindrical holes is a counter-rotating vortex pair (CVP). It originates from the deflection of the coolant entering the hole and typically persists throughout the hole and downstream of the hole exit. Additionally, a separation bubble could form immediately downstream of the sharp turn at the hole inlet, which causes an acceleration of the fluid and a disturbed velocity profile inside the hole ("jetting effect"). Particularly for high blowing ratios the CVP enhances mixing, leading to a faster coolant jet dissipation and entrainment of hot gas underneath the coolant jet, which negatively affects overall cooling effectiveness.

Figure 4 shows the distributions of the streamwise, wall normal and lateral velocity components at constant x planes. The top row represents the experimental results and the bottom row the computational results. The spatial coordinates are normalized with the hole diameter d and the velocity components with the freestream reference velocity u_{ref}, which was measured at a discrete location upstream in the center of the channel (Note the difference in color scales between the velocity components).

The comparison between the experimental and computational results (bottom row) shows very good qualitative agreement for all velocity components. Comparing the streamwise velocities, it can be seen that the experimental approach flow inhomogeneity could not be modeled perfectly, the CFD deviates locally by up to 10% of the reference velocity but for the most part deviations are below 5%. Regarding the exiting jet momentum, the agreement between CFD and experiment is of the same accuracy. A similar jet expansion, velocity distribution as well as velocity magnitudes between the PIV measurements and the computational results can be observed, looking at the bottom row of Figure 4. The lateral velocities underline the quality of the CFD simulation. The aforementioned vortex branches agree well with the experimental results. In the CFD even the lower branches with lateral velocities directed towards the jet center can be seen near the wall.

The left column of Figure 4 shows the streamwise velocity component. A blowing ratio of $M = 1.0$ and a density ratio of

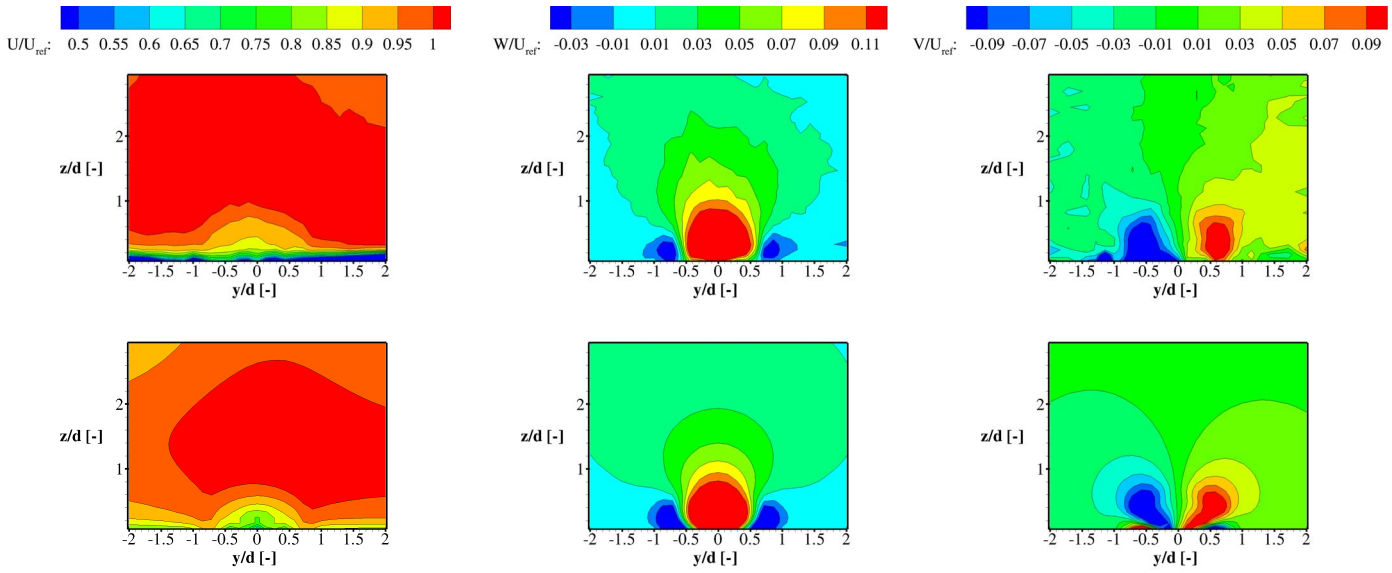

FIGURE 4. Experimental (top) and computational (bottom) distributions of streamwise (left), wall normal (center) and lateral (right) velocity components at $x/d = 1$ for cylindrical hole coolant ejection at $\alpha = 35°$, $M = 1.0$, $DR = 1.4$, $Tu = 7\%$

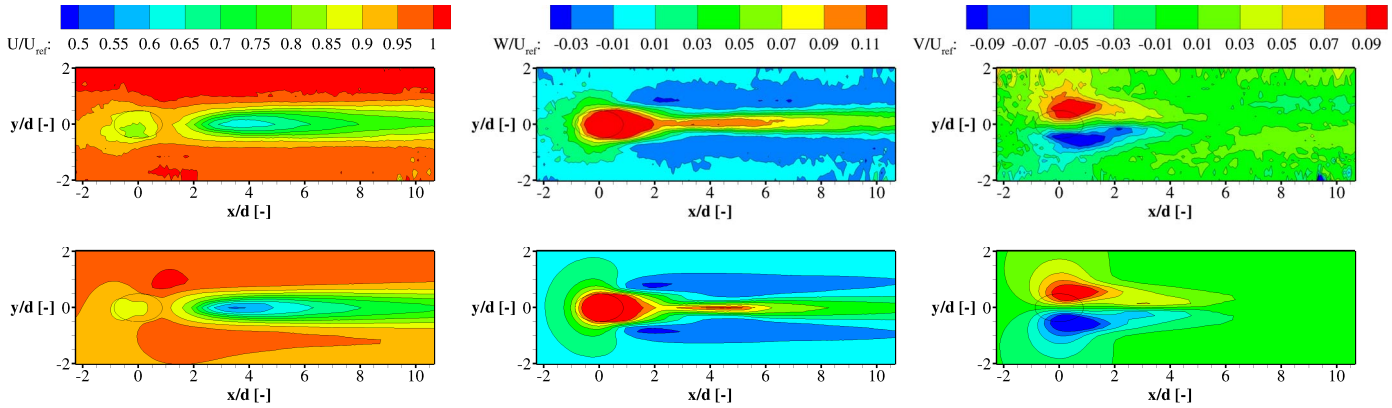

FIGURE 5. Experimental (top) and computational (bottom) distributions of streamwise (left), wall normal (center) and lateral (right) velocity components at $z/d = 0.5$ for cylindrical hole coolant ejection at $\alpha = 35°$, $M = 1.0$, $DR = 1.4$, $Tu = 7\%$

$DR = 1.4$ leads to a velocity ratio between coolant and hot gas of $VR = 0.71$. Thus the exiting jet can be identified by lower velocity magnitudes in comparison to the cross flow. The characteristic CVP is easily recognized in the wall normal velocity distribution in the center column of Figure 4. A high upward momentum can be seen in the jet center whereas a downward momentum exists at the outer jet regions. Looking at the lateral velocity in the right column of Figure 4 allows to identify the individual vortex branches and their direction of rotation. Due to near wall measurement uncertainties of the PIV, only the upper half of the vortex structure is visible in the experimental results. Looking at planes further downstream (not presented in this paper), the lower vortex branches can also be identified in the PIV by a lateral velocity directed towards the jet center in the wall vicinity.

Figure 5 shows the velocity component contours in a plane parallel to the platform at a distance of $z/d = 0.5$ with the hole breakout indicated. Again, the top row represents the experimental data and the bottom row the computational results. The streamwise velocity shows a low velocity region at approximately $x/d = -0.5$ due to the cross flow obstruction by the exiting jet. The low velocity region located along the center line

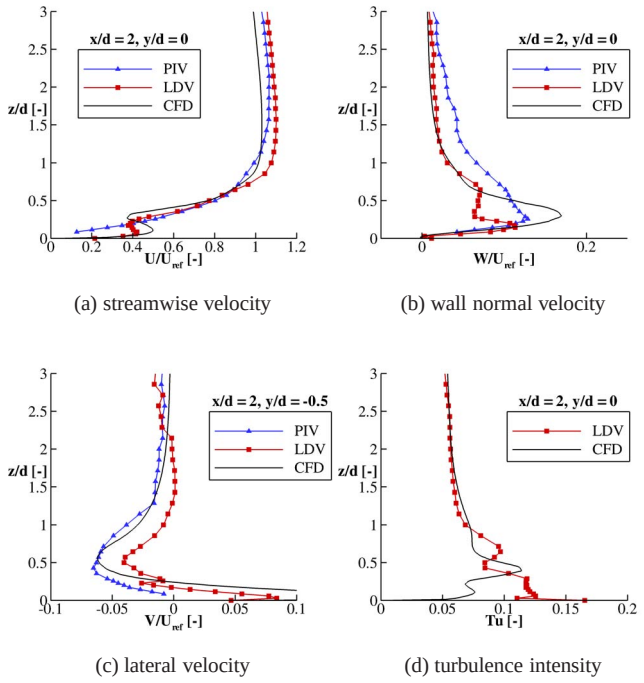

(a) streamwise velocity (b) wall normal velocity

(c) lateral velocity (d) turbulence intensity

FIGURE 6. PIV, LDV, CFD velocity and turb. int. profiles for cylindrical hole coolant ejection at $\alpha = 35°$, $M = 1.0$, $DR = 1.4$, $Tu = 7\%$

at $3d$ to $4d$ downstream of the jet ejection indicates where the jet emerges beyond $z/d = 0.5$. The counter rotating vortex pair can be seen best in the pictures on the right. Looking at the wall normal distribution (center), the downward momentum at the outer jet regions extends far downstream and indicates the persistence of the kidney vortex. It also shows the turning of the film cooling jet due to the crossflow interaction, which takes place from $x/d \approx -1$ to $x/d \approx 1.5$. The streamwise and the wall normal velocity distribution also show the typical jet contraction downstream of cylindrical holes as observed by Walters and Leylek [26]. The computational results (Figure 5, bottom row) confirm the good agreement between simulation and experiment. The extent and location of the predicted low velocity region upstream and downstream of the jet ejection agree very well with the experimental results with quantitative deviations on the order of 5-10% of the reference velocity. Also, the strength and the stability of the kidney vortex is predicted well. This again underlines the capability of the computational model to predict the main flow structures and secondary flows associated with ejection from cylindrical cooling holes.

Figure 6 presents wall-normal profiles for all three velocity components at different locations above the platform (const. *x*,*y*) and the corresponding turbulence intensity profile. The latter was determined from measurements of RMS velocity obtained as part of the LDV measurement campaign. Similar to the presented contour plots, the axes are normalized with the hole diameter d and the velocities with u_{ref}. Blue curves (triangles) represent the profiles extracted from PIV data, red curves (rectangles) the profiles measured by LDV and black curves represent the computational results.

As LDV measurements and CFD show, the near wall velocity profiles are disturbed due to the presence of the coolant jet. Good qualitative agreement between the experimental and computational profiles is noticeable. However, there are some discrepancies in the velocity magnitudes. The CFD overpredicts streamwise velocity in the jet region ($z/d < 0.5$) by $0.05 \ldots 0.1 u_{ref}$ and by $0.02 u_{ref}$ for the secondary flow velocity components on average, with local deviations up to $0.08 u_{ref}$. For the streamwise component, the disturbance due to the jet was not detected by the PIV measurement as it cannot resolve the flow as close to the wall as the LDV measurement method. Considering the wall normal velocity in Figure 6(b) it can be seen that all three curves have similar shapes. The lateral velocity profiles shown in Figure 6(c) are located $-0.5d$ off the centerline so that a vortex branch can be examined, which is detected by both measurements and the CFD. The turbulence intensity profiles of the LDV and CFD in Figure 6(d) show additional turbulence production in the shear layer between cooling air and cross flow at $z/d = 0.7$ and $z/d = 0.5$ for experimental and CFD results respectively. The CFD predicts the shear layer turbulence intensity peak $0.2d$ closer to the wall and with 13% significantly higher than the experiments with approximately 9% only. In contrast, the computational simulation underpredicts the turbulence intensity in wall vicinity ($z/d < 0.5$), most likely due to the predefined constant turbulent length scale at the inlet, based on cross flow mean values, which are not representative for near wall conditions. However the turbulence intensity still matches the LDV data well in terms of upper jet region and main stream, with experiment and CFD predicting turbulence intensities on the order of 5%. PIV data is not available for turbulence intensity.

Laidback Fanshaped Film Cooling Hole

Case 1: $\alpha = 35°$, $M = 1.0$, $DR = 1.4$, $Tu = 7\%$

The first case with a diffuser hole geometry presented in this paper was operated at the same aero-thermodynamic conditions as the cylindrical hole. This allows a direct comparison between a film cooling jet exiting a diffuser hole and a cylindrical hole. A very early investigation of Goldstein et al. [3] showed the advantage of diffuser shaped holes. They observed a reduced momentum of the exiting film cooling jet in comparison to a cylindrical hole due to the increased cross-sectional area. This results in less penetration into the crossflow and less interaction between crossflow and film cooling jet. Thus the interaction is restricted to the wall vicinity and enables coolant ejection with reduced disturbance to the free stream boundary layer. Unlike the cylin-

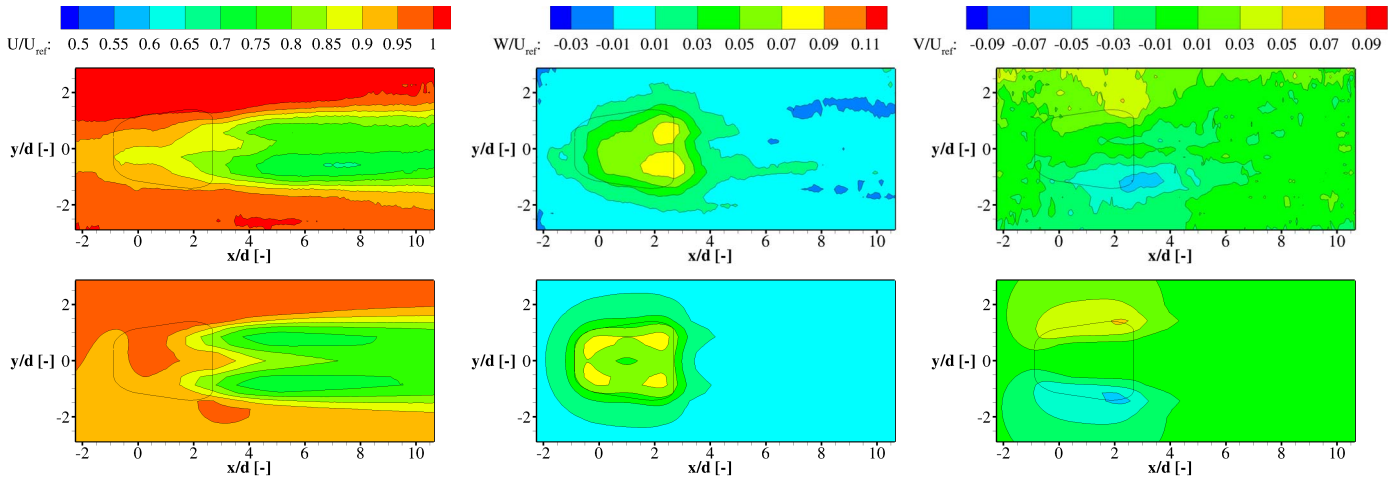

FIGURE 7. Experimental (top) and computational (bottom) distributions of streamwise (left), wall normal (center) and lateral (right) velocity components at $z/d = 0.5$ for diffuser hole coolant ejection at $\alpha = 35°$, $M = 1.0$, $DR = 1.4$, $Tu = 7\%$

drical hole, the characteristic kidney vortex is not the dominating flow structure anymore. Instead, the flow behavior is dominated by lateral spreading due to the diffuser geometry leading to reduced momentum of the film cooling jet. A steady separation zone located at the center of the diffuser directs the coolant flow away from the centerline leading to a jet bifurcation further enhancing the lateral spreading as also observed by Saumweber and Schulz [14] for high area ratio shaped holes.

Results of the PIV measurements are presented in the top row of Figure 7 and show the velocity distribution in a wall parallel plane $0.5z/d$ off the platform. In comparison to the cylindrical hole, there is no low velocity region upstream of the jet ejection due to the weaker penetration into the crossflow. Lateral spreading is increased and lower velocity magnitudes are observed looking at the streamwise velocity component. Both streamwise and wall normal velocity distributions show the characteristic jet bifurcation for a fan shaped diffuser as well as the evident lower exit momentum in comparison to the cylindrical hole. Flow bifurcation leads to two distinguishable streaks of low streamwise velocity at $y/d = \pm 1$ as well as to regions of elevated wall normal velocity separated by a region of lower velocity at $y/d = 0$. Wall normal velocities in the downstream portion of the hole breakout are higher by $0.02u_{ref}$, indicating flow blockage at the upstream edge of the diffuser. This is characteristic for large area ratio diffusers at low blowing ratios due to the very low momentum of the exiting film cooling jet in comparison to the strong crossflow. The contour plot on the right presents the PIV results for the lateral velocity component and underlines the lateral spreading. Opposite to the cylindrical case, no kidney vortex is noticeable.

The bottom row in Figure 7 represents the CFD results. The characteristic flow bifurcation is apparent in both streamwise and

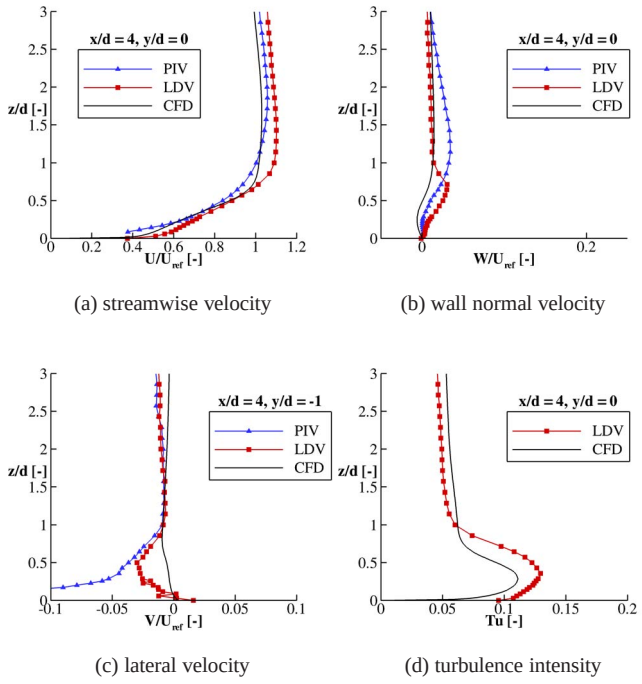

(a) streamwise velocity (b) wall normal velocity

(c) lateral velocity (d) turbulence intensity

FIGURE 8. PIV, LDV, CFD velocity and turb. int. profiles for diffuser hole coolant ejection at $\alpha = 35°$, $M = 1.0$, $DR = 1.4$, $Tu = 7\%$

wall normal velocity distributions. Approximately 10% wider jet expansion downstream can be seen in the computational results for streamwise velocity, but velocity magnitudes and distribution in the jet-affected region are matched within less than 5% of the

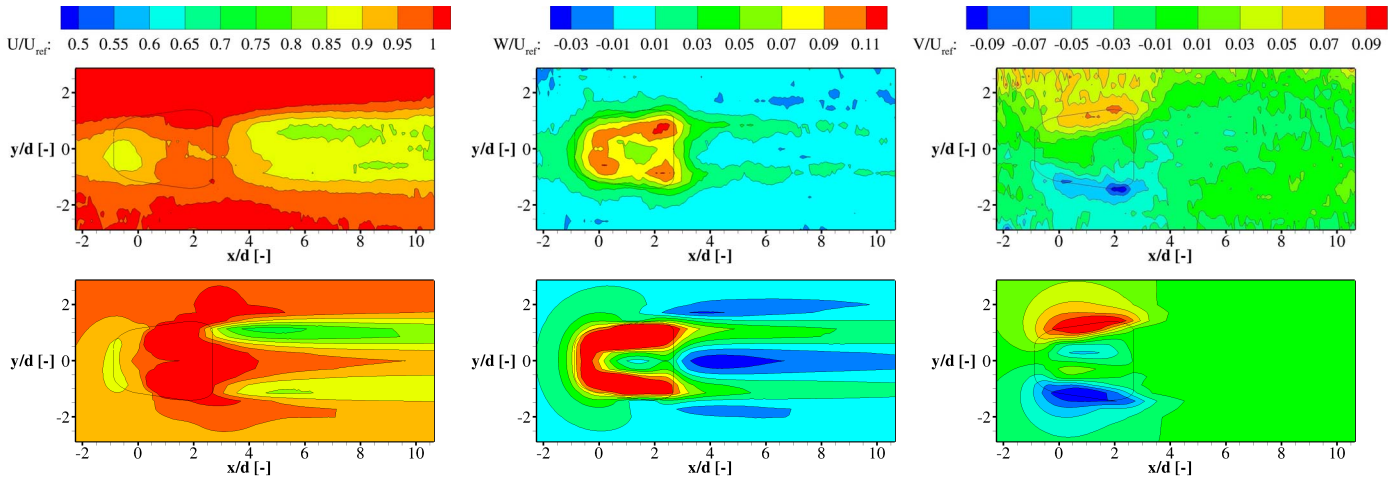

FIGURE 9. Experimental (top) and computational (bottom) distributions of streamwise (left), wall normal (center) and lateral (right) velocity components at $z/d = 0.5$ for diffuser hole coolant ejection at $\alpha = 35°$, $M = 2.0$, $DR = 1.1$, $Tu = 7\%$

reference velocity. Outside of the jet region, streamwise velocities deviate by 5-10% reference velocity due to the issues related to modeling of approach flow inhomogeneity. Considering the wall normal component, higher velocities in the upstream half of the hole breakout indicate underpredicted flow blockage. This tendency of the CFD will become more obvious when considering the high blowing ratio case for the diffuser hole. However, the bifurcation due to the recirculation region inside the diffuser is resolved and the disagreement between the PIV and CFD data attenuates further downstream. In comparison to the PIV data for the lateral velocity, the CFD shows the same tendencies. The film cooling jet is pushed to the diffuser side walls and directed further downstream by the diffuser edges. Similar to the wall normal velocity component, the velocity magnitudes are slightly higher for the computations compared to the experimental results. One possible explanation might be an overprediction of the separation bubble inside the diffuser.

Figure 8 presents PIV, LDV and CFD profiles for the three velocity components and the turbulence intensity. The minimal disturbance of the streamwise velocity profile due to the reduced momentum of the film cooling jet is reflected by both the experimental and computational results. Looking at the wall normal velocity component, lower velocity magnitudes compared to the cylindrical case are noticeable. The good agreement among the three curves in terms of shape and magnitudes is evident. However, the profiles confirm the tendency of slightly higher predicted velocities for secondary flow in the CFD simulation. Due to the noisy data a lateral component is noticeable for the PIV, whereas the CFD and LDV show no lateral omponent. The turbulence production in the jet-affected region is underpredicted by about 20% in the CFD but shows a similiar shape in comparison to the LDV curve.

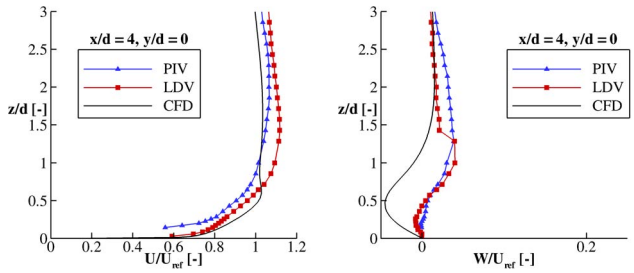

(a) streamwise velocity (b) wall normal velocity

FIGURE 10. PIV, LDV, CFD velocity profiles for diffuser hole coolant ejection at $\alpha = 35°$, $M = 2.0$, $DR = 1.1$, $Tu = 7\%$

Case 2: $\alpha = 35°$, $M = 2.0$, $DR = 1.1$, $Tu = 7\%$

The second case with a diffuser geometry was operated with a density ratio of 1.1, a turbulence intensity of 7% and a blowing ratio of 2.0. For a cylindrical hole a blowing ratio this high would definitely cause the coolant jet to lift off from the wall. As mentioned earlier, this would lead to an increased dissipation and a substantially reduced cooling effectiveness. However, for diffuser holes, one can observe an increased cooling effectiveness for higher blowing ratios (cp. [15]). Due to the reduced momentum at the exit, the jet does not lift off and remains attached to the wall. Combined with the higher coolant mass flow and improved lateral spreading, an increased overall cooling effectiveness can be achieved. However higher velocites and a more pronounced jet bifurcation are expected leading to a wider lateral spreading in comparison to the diffuser operated with a blowing ratio of $M = 1.0$.

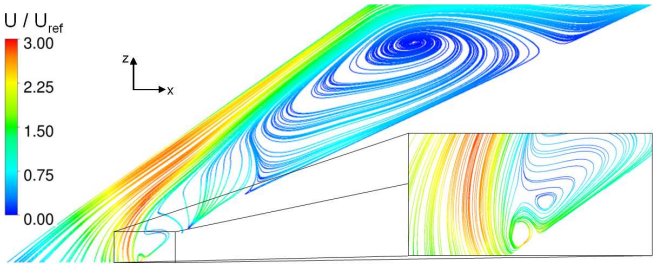

FIGURE 11. CFD streamlines in diffuser hole at $y/d = 0$, $M = 2.0$

The PIV measurements are presented in the same manner as for the previous cases in the top row of Figure 9. In general, higher velocities in comparison to the lower blowing ratio are observed for all three velocity components. The streamwise velocity shows a slight deceleration upstream of the hole exit ($x/d \approx -0.5$) but it is not as pronounced as for the cylindrical hole. As expected, the wall normal component shows a strong jet bifurcation with a recirculation region in the middle of the diffuser, which is qualitatively similar to the CFD result for the low blowing ratio case (Figure 7).

There are significant discrepancies when comparing the PIV measurements with the computational results. Considering the streamwise velocity component, an asymmetric distribution is predicted. Furthermore velocity magnitudes for wall-normal and lateral velocity are significantly overpredicted. The wall normal velocity still shows a jet bifurcation but overpredicts the recirculation region, which leads to an accelerated jet towards the upstream diffuser wall and side walls. The lateral velocity shows the expected distribution but again with higher velocity magnitudes in comparison to the PIV measurements.

Figure 10 shows the profiles of streamwise and wall normal velocity. A slightly disturbed wall normal velocity profile near the wall can be seen for the experimental data whereas the CFD curve underlines the tendency of overprediction and shows a significant disagreement compared to LDV and PIV data. The discrepancy of the streamwise component is not as significant as for the wall-normal component at this position.

Non-convergence can be excluded as a reason for the asymmetric velocity distribution. Since the flow is most likely unsteady, the authors assume that using a pseudo-time stepping scheme as implemented in ANSYS CFX to force a steady solution on this inherently unsteady flow tends to deliver rather a snapshot of the unsteady flow field than a true steady result. A time averaged solution would probably show a more symmetric solution but was not investigated in the scope of this paper.

The reason for the high velocities, particular for the diffuser with a high blowing ratio, is assumed to be an overprediction of the separation inside the diffuser. A comparison of the pressure loss over the diffuser revealed losses up to 50% higher for the CFD calculations relative to the experiments. This can be interpreted as a sign for an overpredicted separation.

Figure 11 shows a cut at $y/d = 0$ through the diffuser with streamlines obtained from the CFD solution. A small bubble of recirculating flow can be seen right after the hole inlet due to the sharp turning, which leads to the characteristic jetting effect. Downstream of the separation bubble a fraction of the coolant flow reattaches, forming a small counter-rotating vortex (see magnified section of Figure 11) followed by a region of low velocity fluid that spans more than half of the hole's cross-section. The majority of the coolant mass flow remains in the jetting region close to the upstream wall of the cooling hole. The flow again separates right after the beginning of the diffuser section. The large and probably overpredicted size of this second separation bubble prevents deceleration of the jet, making the diffuser ineffective due to a contraction of the effective cross section. This results in a high momentum cooling jet exiting the film cooling hole. Using the reattachment modification of the k-ω-SST turbulence model [47] reduced the size of the separation region, but still overpredicts it.

Cooling Effectiveness

Figure 12 shows a chart of the laterally averaged film cooling effectiveness for the cylindrical hole and the diffuser hole at a blowing ratio of $M = 1.0$. Both, experimental and computational results are included in the chart along with experimental data for cylindrical holes at similar boundary conditions by Pedersen et al. [48] and Baldauf et al. [49]. The data from the present study agrees well with the reference data. Baldauf et al. [49] used a more shallow inclination angle of 30° and therefore measured higher cooling effectiveness. Note that film cooling effectiveness was normalized by the geometric hole coverage t/P, which is significantly larger for the diffuser hole than for the cylindrical hole. Results are given in a streamwise range of $5 < x/D < 26$ which corresponds to the analyzable extension of the near adiabatic test plate. The shown chart underlines the superior cooling behavior of the laidback fan shaped diffuser in comparison to a cylindrical hole geometry. As mentioned before the reduced exit momentum and increased lateral spreading lead to a better coverage of the platform and increases the laterally averaged cooling effectiveness. Note that these single hole ejection results cannot be compared with row injection data.

The comparison of thermographic measurement results and CFD predictions show a good agreement particularly for the cylindrical case. An almost constant low level for the cylindrical case can be observed while the effectiveness decay for the shaped hole is more pronounced but on a much higher effectiveness level. The superior cooling effectiveness of the shaped hole geometry is evident and up to three times higher than the effectiveness for the cylindrical hole. This underlines again the faster dissipation and mixing of the cooling jet exiting a cylindrical hole, which appears to happen intensively within five diam-

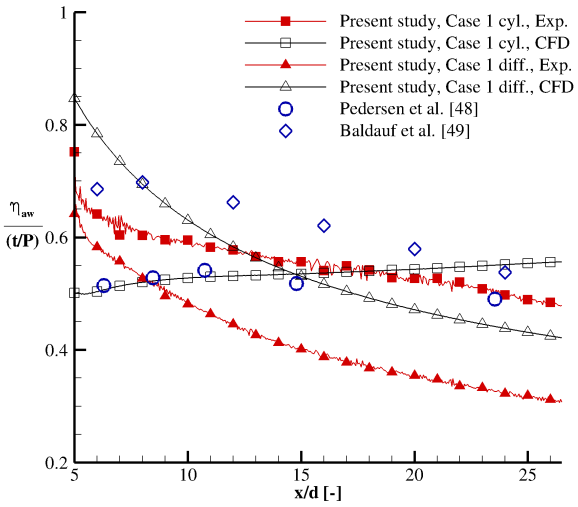

FIGURE 12. Laterally averaged cooling effectiveness for cylindrical and diffuser hole at $M = 1.0$

eters after the jet ejection and would explain its almost constant low level of cooling effectiveness. The disagreement between the computational and experimental result for the diffuser geometry can partially be attributed to the deviations already observed in the aerodynamic results. Additionally, the heat exchange inside the hole, which leads to higher coolant temperatures at the hole exit is not accounted for in the truly adiabatic CFD calculations. A further reason is the underprediction of the turbulent lateral diffusion in the CFD due to the use of an isotropic turbulence model. This well known issue leads to an overprediction of the centerline cooling effectiveness and to slower effectiveness decay, which leads to higher laterally averaged values. However, the slope of the effectiveness curve is predicted quite well by the CFD.

CONCLUSION

3D PIV and LDV flow field measurements for a cylindrical film cooling hole and a laidback fan shaped diffuser at two operating points were presented in this paper. Infrared thermography measurements were conducted to determine the film cooling effectiveness. The results were compared to detailed CFD calculations.

A very good agreement between experiments and CFD simulation could be achieved for the cylindrical hole. Velocity distribution and magnitudes as well as jet expansion and secondary flow matched the experimental results persuasively. Good qualitative agreement but locally significant quantitative deviations were observed for the diffuser hole operated with the same boundary conditions (low blowing ratio of 1.0). Deviations of the wall normal velocity and jet expansion were recognized but in general the flow field is predicted quite well. A significant disagreement could be seen for the higher blowing ratio case. Much higher velocity magnitudes and asymmetric distributions occurred in the CFD calculations. The flow field is strongly affected by a separation bubble inside the diffuser, which appears to be overpredicted by the CFD. This error is more pronounced at higher blowing ratios. However, the characteristic flow structures, namely the flow bifurcation, were predicted correctly despite deviations in velocity magnitudes for increased blowing ratios. No explanation was found for the asymmetric distribution yet, but is assumed to be due to the inherently unsteady character of the flow. Considering cooling effectiveness the level of effectiveness is predicted well for the cylindrical case, but the shape of the curve is not, whereas for the diffuser case the shape of the effectiveness curve is predicted very well, but the level is overpredicted.

ACKNOWLEDGMENT

The authors would like to thank Prof. Dr. Michael Crawford and Dr. Andreas Heselhaus for sharing their heat transfer expertise. Thanks to Prof. Dr. Konrad Vogeler from TU Dresden for his support of this work and for the academic supervision of Mr. Torsten Sämel's Diploma Thesis.

PERMISSION FOR USE

REFERENCES

[1] Goldstein, R. J., Eckert, E. R. G., and Ramsey, J. W., 1968. "Film Cooling With Injection Through Holes: Adiabatic Wall Temperatures Downstream of a Circular Hole". *J. Eng. Power,* ***90***, pp. 384–395.

[2] Goldstein, R. J., Eckert, E. R. G., Eriksen, V. L., and Ramsey, J. W., 1970. "Film Cooling Following Injection Through Inclined Circular Tubes". *Israel J. Technol.,* ***8***, pp. 145–154.

[3] Goldstein, R. J., Eckert, E. R. G., and Burggraf, F., 1974. "Effects of Hole Geometry and Density on Three-Dimensional Film Cooling". *Int. J. Heat Mass Tran.,* ***17***, pp. 595–607.

[4] Foster, N. W., and Lampard, D., 1980. "The Flow and Film Cooling Effectiveness Following Injection Through a Row of Holes". *J. Eng. Power,* ***102***, pp. 584–588.

[5] Baldauf, S., Schulz, A., and Wittig, S., 2001. "High Resolution Measurements of Local Heat Transfer Coefficients by

Discrete Hole Film Cooling". *J. Turbomach.,* ***123***, pp. 749–755.
[6] Baldauf, S., Schulz, A., and Wittig, S., 2001. "High Resolution Measurements of Local Effectiveness by Discrete Hole Film Cooling". *J. Turbomach.,* ***123***, pp. 758–765.
[7] Schmidt, D. L., Sen, B., and Bogard, D., 1996. "Film Cooling with Compound Angle Holes: Adiabatic Effectiveness". *J. Turbomach.,* ***118***, pp. 807–813.
[8] Ligrani, P., Wigle, J. M., and Jackson, S., 1994. "Film-Cooling from Holes with Compound Angle Orientations: Part 2 - Results Downstream of a Single Row of Holes with 6d Spanwise Spacing". *J. Heat Trans.,* ***116***, pp. 353–362.
[9] Goldstein, R. J., and Jin, P., 2000. "Film Cooling Downstream of a Row of Discrete Holes with Compound Angle". ASME Paper No. 2000-GT-248.
[10] Lutum, E., and Johnson, B. V., 1998. "Influence of the Hole Length-to-Diameter Ratio on Film Cooling with Cylindrical Holes". ASME Paper No. 98-GT-10.
[11] Burd, S. W., Kaszeta, R. W., and Simon, T. W., 1998. "Measurements in Film Cooling Flows: Hole L/D and Turbulence Intensity Effects". *J. Turbomach.,* ***120***, pp. 791–798.
[12] Bunker, R., 2005. "A Review of Shaped Hole Turbine Film-Cooling Technology". *J. Heat Trans.,* ***127***, pp. 441–453.
[13] Gritsch, M., Schulz, A., and Wittig, S., 1997. "Adiabatic Wall Effectiveness Measurements of Film-Cooling Holes with Expanded Exits". 42nd Annual International Gas Turbine and Aeroengine Congress and Exposition.
[14] Saumweber, C., and Schulz, A., 2008. "Effect of Geometry Variations on the Cooling Perfomance of Fan-Shaped Cooling Holes". ASME Paper No. GT2008-51038.
[15] Gritsch, M., Colban, W., Schär, H., and Döbbeling, K., 2005. "Effect of Hole Geometry on the Thermal Performance of Fan-Shaped Film Cooling Holes". *J. Turbomach.,* ***127***, pp. 718–725.
[16] Heneka, C., Schulz, A., Bauer, H.-J., Heselhaus, A., and Crawford, M. E., 2010. "Film Cooling Performance of Sharp-Edged Diffuser Holes with Lateral Inclination". ASME Paper No. GT2010-23090.
[17] Pietrzyk, J. R., Bogard, D. G., and Crawford, M. E., 1989. "Hydrodynamic Measurements of Jets in Crossflow for Gas Turbine Film Cooling Applications". *J. Turbomach.,* ***111***, pp. 139–145.
[18] Thole, K. A., Gritsch, M., Schulz, A., and Wittig, S., 1998. "Flowfield Measurements for Film-Cooling Holes With Expanded Exits". *J. Turbomach.,* ***120***, pp. 327–336.
[19] Lee, S. W., Lee, J. S., and Ro, S. T., 1994. "Experimental Study on the Flow Characteristics of Streamwise Inclined Jets in Crossflow on Flat Plate". *J. Turbomach.,* ***116***, pp. 97–105.
[20] Lee, S. W., Kim, Y. B., and Lee, J. S., 1997. "Flow Characteristics and Aerodynamic Losses of Film-Cooling Jets with Compound Angle Orientations". *J. Turbomach.,* ***119***, pp. 310–319.
[21] Jessen, W., Schröder, W., and Klaas, M., 2007. "Evolution of Jets Effusing from Inclined Holes into Crossflow". *Int. J. Heat Fluid Fl.,* ***28***, pp. 1312–1326.
[22] Jessen, W., Konopka, M., and Schröder, W., 2010. "Particle-Image Velocimetry Measurements of Film Cooling in an Adverse Pressure Gradient Flow". ASME Paper No. GT2010-22411.
[23] Kercher, D., 1998. "A Film-Cooling CFD Bibliography: 1971-1996". *Int. J. Rot. Mach.,* ***4***, pp. 61–72.
[24] Leylek, J., and Zerkle, R., 1994. "Discrete-Jet Film Cooling: A Comparison of Computational Results With Experiments". *J. Turbomach.,* ***116***, pp. 358–368.
[25] Walters, D., and Leylek, J., 1997. "A Systematic Computational Methodology Applied to a Three-Dimensional Film-Cooling Flowfield". *J. Turbomach.,* ***119***, pp. 777–785.
[26] Walters, D., and Leylek, J., 2000. "A Detailed Analysis of Film Cooling Physics: Part I - Streamwise Injection with Cylindrical Holes". *J. Turbomach.,* ***122***, pp. 102–108.
[27] Hyams, D., and Leylek, J., 2000. "A Detailed Analysis of Film Cooling Physics: Part III - Streamwise Injection With Shaped Holes". *J. Turbomach.,* ***122***, pp. 122–132.
[28] Bacci, A., and Facchini, B., 2007. "Turbulence Modeling for the Numerical Simulation of Film and Effusion Cooling Flows". ASME Paper No. GT2007-27182
[29] Shih, T. I.-P., and Na, S., 2007. "Momentum-Preserving Shaped Holes for Film Cooling". ASME Paper No. GT-2007-27600.
[30] Na, S., and Shih, T. I.-P., 2007. "Increasing Adiabatic Film-Cooling Effectiveness by Using an Upstream Ramp". *J. Heat Trans.,* ***129***, April, pp. 464–471.
[31] Lee, K.-D., and Kim, K.-Y., 2009. "Optimization of a Fan-Shaped Hole for Film Cooling Using a Surrogate Model". ASME Paper No. GT2009-59520.
[32] Kissel, H. P., Weigand, B., von Wolfersdorf, J., Neumann, S. O., and Ungewickell, A., 2007. "An Experimental and Numerical Investigation of the Effect of Cooling Channel Crossflow on Film Cooling Performance". ASME Paper No. GT2007-27102
[33] Colban, W., Thole, K., and Händler, M., 2007. "Experimental and Computational Comparisons of Fan-Shaped Film Cooling on a Turbine Vane Surface". *J. Turbomach.,* ***129***, pp. 23–31.
[34] Goormans-Francke, C., Carabin, G., and Hirsch, C., 2008. "Mesh Generation for Conjugate Heat Transfer Analysis of a Cooled High Pressure Turbine Stage". ASME Paper No. GT2008-50660.
[35] Miller, K. L., and Crawford, M. E., 1984. "Numerical Simulation of Single, Double, and Multiple Row Film Cooling Effectiveness and Heat Transfer". ASME Paper No. 84-GT-112.
[36] Heidmann, J. D., and Hunter, S. D., 2001. Coarse Grid

Modeling of Turbine Film Cooling Flows Using Volumetric Source Terms. Technical Report No. NASA/TM-2001-210817.
[37] Burdet, A., Abhari, R. S., and Rose, M. G., 2005. "Modeling of Film Cooling - Part II: Model for Use in 3D CFD". ASME Paper No. GT2005-68780.
[38] Tartinville, B., and Hirsch, C., 2008. "Modelling of Film Cooling for Turbine Blade Design". ASME Paper No. GT2008-50316.
[39] auf dem Kampe, T. G., and Völker, S., 2010. "A Model for Cylindrical Hole Film Cooling: Part II - Model Formulation, Implementation and Results". ASME Paper No. GT2010-22788.
[40] auf dem Kampe, T. G., and Völker, S., 2009. "A Correlation-Based Methodology to Predict the Flow Structure of Flows Emanating from Cylindrical Holes with Application to Film Cooling". Proc. International Symposium on Heat Transfer in Gas Turbine Systems, Antalya.
[41] auf dem Kampe, T. G., Zehe, F. N., and Völker, S., 2010. "A Model for Cylindrical Hole Film Cooling: Part I - A Correlation for Jet-Flow with Application to Film Cooling". ASME Paper No. GT2010-22787.
[42] Kays, W., Crawford, M., and Weigand, B., 2004. Convective Heat and Mass Transfer. McGraw Hill Higher Education.
[43] Martiny, M., Schiele, R., Gritsch, M., Schulz, A., and Wittig, S., 1997. "In Situ Calibration for Quantitative Infrared Thermography". *Eurotherm S.,* ***50***, pp. 3–8.
[44] Schulz, A., 2000. "Infrared Thermography as Applied to Film Cooling of Gas Turbine Components". *Meas. Sci. Technol.,* ***11***, pp. 1–9.
[45] Ochs, M., Horbach, T., Schulz, A., Koch, R., and Bauer, H.-J., 2009. "A Novel Calibration Method for an Infrared Thermography System Applied to Heat Transfer Experiments". *Meas. Sci. Technol.,* ***20***, pp. 9–17.
[46] Kline, S., and McClintock, F., 1953. "Describing Uncertainties in Single-Sample Experiments". *Mech. Eng.,* ***75***(1), pp. 3–8.
[47] Menter, F., 1994. "Two-Equation Eddy-Viscosity Turbulence Models for Engineering Applications". *AIAA J.,* ***32***, pp. 1598–1605.
[48] Pedersen, D. R., Eckert, E. R. G., and Goldstein, R. J., 1977. "Film Cooling With Large Density Differences Between the Mainstream and the Secondary Fluid Measured by the Heat-Mass Transfer Analogy". *J. Heat Trans.,* ***99***, pp. 620–627.
[49] Baldauf, S., Scheurlen, M., Schulz, A., and Wittig, S., 2002. "Correlation of Film-Cooling Effectiveness From Thermographic Measurements at Enginelike Conditions". *J. Turbomach.,* ***124***, pp. 686–698.

